New aspect-ratio effect in three-component composites for piezoelectric sensor, hydrophone and energy-harvesting applications

V.Yu. Topolov[a,]*, C.R. Bowen[b] and P. Bisegna[c]

[a]*Department of Physics, Southern Federal University, 5 Zorge Street, 344090 Rostov-on-Don, Russia*

[b]*Department of Mechanical Engineering, University of Bath, Bath BA2 7AY, UK*

[c]*Department of Civil Engineering and Computer Science, University of Rome "Tor Vergata", 00133 Rome, Italy*

ABSTRACT In this paper the influence of the aspect ratio of ferroelectric ceramic inclusions on the piezoelectric performance and hydrostatic parameters of novel three-component 1–3-type composites based on a relaxor-ferroelectric single crystals is studied. Differences in the microgeometry of the ceramic/polymer matrix with 0–3 connectivity and the presence of two piezo-active components with contrasting piezoelectric and mechanical properties lead to a considerable dependence of the aspect ratio and volume fraction of the aligned ceramic inclusions on the piezoelectric performance, hydrostatic response and related parameters of the 1–0–3 composite. The influence of the elastic anisotropy of the ceramic/polymer matrix on composite properties with changes in the aspect ratio and volume fraction of the inclusions is discussed. The piezoelectric performance of the 1–0–3 $0.67Pb(Mg_{1/3}Nb_{2/3})O_3$–$0.33PbTiO_3$ single crystal/modified $PbTiO_3$ ceramic/polymer composite suggests that such a material is of interest for both sensor and energy-harvesting applications due to large values of the piezoelectric coefficient g_{33}^*≈400–550 mV·m/N, squared figure of merit $d_{33}^*\, g_{33}^*$~10^{-10}Pa^{-1} and related anisotropy factor $d_{33}^*\, g_{33}^*/(d_{31}^*\, g_{31}^*)$≈8–9. Such composites can also be used in hydrophone applications due to their large hydrostatic parameters, e.g., d_h^*~10^2 pC/N, g_h^*≈100–160 mV·m/N and $d_h^*\, g_h^*$~10^{-11} Pa^{-1}.

Keywords: piezo-active composite; relaxor-ferroelectric single crystal; ferroelectric ceramic; polymer; piezoelectric sensitivity

*Corresponding author. Tel.:+7 8632975127; fax:+7 8632975120, E-mail: vutopolov@sfedu.ru

1. Introduction

There is a continued interest in advanced piezo-active composites based on relaxor-ferroelectric single crystals (SCs) [1–4] as a result of the high piezoelectric activity of the SC component [5–8] and polarisation orientation effects [3]. This makes such composites attractive for a variety of important piezotechnical applications, such as sensing and energy harvesting [9]. Of particular interest are relaxor-ferroelectric SC/polymer composites [1–3] with 1–3 connectivity in terms of the work of Newnham et al. [10]. SCs of perovskite-type relaxor-ferroelectric solid solutions of $(1–x)Pb(Mg_{1/3}Nb_{2/3})O_3–xPbTiO_3$ (PMN–*x*PT) and $(1– x)Pb(Zn_{1/3}Nb_{2/3})O_3–xPbTiO_3$ with engineered domain structures [5,6,8] exhibit high piezoelectric coefficients d_{3j}~10^3 pC/N (see, e.g., Table 1), large electromechanical coupling factors k_{3j} etc. and are therefore strong candidates as highly effective components for modern 1–3 composites [1,2]. A 1–3 composite architecture, which consists of a system of long parallel SC rods in a continuous polymer matrix, can be further modified by the formation of either pores or a system of inclusions in the polymer matrix [11–13]. This additional approach to varying the composite architecture opens up a variety of new methods to tailor the electromechanical coupling, piezoelectric and other characteristics of this composite.

The stimulus for this study of composites based on relaxor-ferroelectric SC is to examine the ability to tailor the effective electromechanical properties of the heterogeneous matrix [12,13] and to optimise specific parameters of the composite [11]. In our opinion, the potential of further improvements of the piezo-composite performance is associated with the influence of the aspect ratio of the inclusions within the two-component matrix on the effective electromechanical properties of a three-component composite. Earlier work has studied the *aspect-ratio effect* in 1–3 [14,15], 2–2 [16] and 0–3 [17] composites based on ferroelectric ceramics (FCs). In these simple two-component composites the geometric sizes of FC rods (1–3 connectivity) relative to the size of the surrounding polymer matrix, geometric sizes of the FC and polymer layers (2–2 connectivity)

and ratios of semi-axes of spheroidal FC inclusions (0–3 connectivity) were varied. However, to the best of our knowledge, no publication has examined the aspect-ratio effect in three-component composites that contain relaxor-ferroelectric SC, FC and polymer, i.e., three kinds of components that are suitable for the manufacture of advanced piezo-composites. The aim of the present paper is to describe and provide a detailed analysis of a *new aspect-ratio inclusion effect* in 1–3-type composites, wherein a 0–3 FC/polymer matrix with variable properties plays an important role in tailoring the composite properties, and to show the performance of this composite in the context of specific piezotechnical applications such as sensors, hydrophones and energy harvesting.

2. Model concept and effective parameters

It is assumed that the three-component composite consists of long relaxor-ferroelectric SC rods embedded in a FC/polymer matrix (Fig.1,a). The SC rods are in the form of a rectangular parallelepiped with square cross sections in the (X_1OX_2) plane, whose centres are arranged into a square array (Fig.1,b). The spontaneous polarisation of each rod is characterised by $\boldsymbol{P}_s^{(1)}||OX_3$. The main crystallographic axes of each rod are oriented as follows: X$||OX_1$, Y$||OX_2$ and Z$||OX_3$. The shape of each FC inclusion in the FC/polymer matrix (see inset in Fig.1,a) obeys the equation $(x_1/a_1)^2+(x_2/a_2)^2+(x_3/a_3)^2=1$ relative to the axes of the rectangular co-ordinate system ($X_1X_2X_3$), where a_1, $a_2=a_1$ and a_3 are the semi-axes of the inclusion, and $\rho_i=a_1/a_3$ is its aspect ratio. We consider the polymer matrix to contain a system of aligned FC inclusions that occupy sites of a simple tetragonal lattice with unit-cell vectors parallel to the OX_k axes, i.e., a regular arrangement of the inclusions in the FC/polymer matrix is observed as shown in Fig.1,c. Examples of meshes, that are used in finite element modelling applied to the FC/polymer matrix, are shown in Fig.1,d,e. The remanent polarisation vector of each FC inclusion is $\boldsymbol{P}_r^{(2)}\uparrow\uparrow OX_3$, and OX_3 is the poling axis of both the matrix and the composite.

The three-component composite (Fig.1,a) is characterised by 1–0–3 connectivity, and the matrix (Fig.1,c) is characterised by 0–3 connectivity in terms of work of Newnham et al. [10]. Manufacturing methods to form the 0–3 matrix, consisting of inclusions in a polymer medium, include electric-field structuring [18] and rapid prototyping [9]. Methods to form the 1–0–3 composite architecture include the use of rod placement using a rod fixture [2,9,19] for the independent preparation of a system of fixed aligned rods with a wide volume-fraction range and the preparation of the heterogeneous matrix with through holes for the long rods [20]. We add that the independent preparation of the rods and matrix has been previously successfully employed, for instance, to a three-component 1–3–1 composite based on FC [20].

Assuming that the linear sizes of the inclusions in the 0–3 matrix are much smaller than the length of the side of the square rod cross section in the (X_1OX_2) plane (Fig.1,a), we evaluate the effective electromechanical properties of the 1–0–3 composite in two stages.

First, the effective electromechanical properties of the 0–3 FC/polymer composite (see inset in Fig.1,a) are represented in the matrix form as $\left\| C^{(m)} \right\| = \begin{pmatrix} ||c^{(m),E}|| & ||e^{(m)}||^t \\ ||e^{(m)}|| & -||\varepsilon^{(m),\xi}|| \end{pmatrix}$, where $||c^{(m),E}||$, $||e^{(m)}||$ and $||\varepsilon^{(m),\xi}||$ are matrices of the elastic moduli (at electric field E=const), piezoelectric coefficients and dielectric permittivities (at mechanical strain ξ=const), respectively, and the superscript 't' denotes the transposition. Taking into account the electromechanical interaction between the piezo-active (poled FC) inclusions, the effective properties of the 0–3 composite are determined by means of the effective field method (EFM) [3]. Following the EFM, we write the matrix of the effective properties of the 0–3 FC/polymer composite as $||C^{(m)}||=||C^{(2)}||+m_i(||C^{(1)}||-||C^{(2)}||)\cdot[||I||+(1-m_i)||S||\cdot||C^{(2)}||^{-1}\cdot(||C^{(1)}||-||C^{(2)}||)]^{-1}$,where superscript '(1)' refers to FC, '(2)' refers to polymer, $||I||$ is the identity matrix, and $||S||$ is the matrix that contains the Eshelby tensor components [3,17] depending on the elements of $||C^{(2)}||$ and the aspect ratio ρ_i. The EFM approach is applicable to the

0–3 composite [3] at relatively small volume fractions of inclusions (e.g., often $m_i < 1/3$ for spherical inclusions and $m_i < 1/2$ for highly prolate inclusions).

An alternative method to determine the effective properties of the heterogeneous matrix is the use of the finite element method (FEM) [3,21] with different meshes of the 0–3 composite structure (see, e.g., Fig.1,d,e). Applying either the EFM or FEM, we find that $||C^{(m)}||=||C^{(m)}(m_i,\rho_i)||$ for the 0–3 FC/polymer matrix.

Second, after the effective electromechanical properties of the 0–3 matrix are determined, the effective properties of the 1–3-type composite with planar interfaces (Fig.1,a), that separate the SC rod and surrounding matrix, are evaluated using the matrix method [3]. Hereby we average the electromechanical properties of the SC rod and 0–3 matrix in the OX_1 and OX_2 directions, in which the periodic structure of the composite is observed, and take into account electromechanical interactions in a 'piezo-active rods–piezo-active matrix' system. Following the matrix method, we represent the effective properties of the 1–0–3 composite in ($X_1X_2X_3$) as

$$||K^*||=||K^*(r,m_i,\rho_i)||=[||K^{(SC)}||\cdot||M||r+||K^{(m)}||(1-r)]\cdot[||M||r+||I||(1-r)]^{-1}. \quad (1)$$

In Eq.(1) $||K^{(SC)}||=\begin{pmatrix} || s^{(SC),E} || & || d^{(SC)} ||^t \\ || d^{(SC)} || & || \varepsilon^{(SC),\sigma} || \end{pmatrix}$ and $||K^{(m)}||=\begin{pmatrix} || s^{(m),E} || & || d^{(m)} ||^t \\ || d^{(m)} || & || \varepsilon^{(m),\sigma} || \end{pmatrix}$ are 9×9 matrices of the electromechanical properties of the SC rod and the 0–3 matrix, respectively, $||M||$ is used to take into account the electric and mechanical boundary conditions [3] at interfaces x_1=const and x_2=const (Fig.1,a), and $||I||$ is the 9×9 identity matrix. For instance, the boundary conditions at x_1=const (Fig.1,a) imply a continuity of components of mechanical stress $\sigma_{11}=\sigma_1$, $\sigma_{12}=\sigma_6$ and $\sigma_{13}=\sigma_5$, strain $\xi_{22}=\xi_2$, $\xi_{23}=\xi_4/2$ and $\xi_{33}=\xi_3$, electric displacement D_1, and electric field E_2 and E_3. The $||M||$ matrix is written for x_1=const in the general form (for an arbitrary symmetry class) as $||M|| = ||\mu_{SC}||^{-1}||\mu_m||$ [3] where

$$\| \mu_{SC} \| = \begin{pmatrix} 1 & 0 & 0 & 0 & 0 & 0 & 0 & 0 & 0 \\ s_{12}^{(SC),E} & s_{22}^{(SC),E} & s_{23}^{(SC),E} & s_{24}^{(SC),E} & s_{25}^{(SC),E} & s_{26}^{(SC),E} & d_{12}^{(SC)} & d_{22}^{(SC)} & d_{32}^{(SC)} \\ s_{13}^{(SC),E} & s_{23}^{(SC),E} & s_{33}^{(SC),E} & s_{34}^{(SC),E} & s_{35}^{(SC),E} & s_{36}^{(SC),E} & d_{13}^{(SC)} & d_{23}^{(SC)} & d_{33}^{(SC)} \\ s_{14}^{(SC),E} & s_{24}^{(SC),E} & s_{34}^{(SC),E} & s_{44}^{(SC),E} & s_{45}^{(SC),E} & s_{46}^{(SC),E} & d_{14}^{(SC)} & d_{24}^{(SC)} & d_{34}^{(SC)} \\ 0 & 0 & 0 & 0 & 1 & 0 & 0 & 0 & 0 \\ 0 & 0 & 0 & 0 & 0 & 1 & 0 & 0 & 0 \\ d_{11}^{(SC)} & d_{12}^{(SC)} & d_{13}^{(SC)} & d_{14}^{(SC)} & d_{15}^{(SC)} & d_{16}^{(SC)} & \varepsilon_{11}^{(SC),\sigma} & \varepsilon_{12}^{(SC),\sigma} & \varepsilon_{13}^{(SC),\sigma} \\ 0 & 0 & 0 & 0 & 0 & 0 & 0 & 1 & 0 \\ 0 & 0 & 0 & 0 & 0 & 0 & 0 & 0 & 1 \end{pmatrix}$$

is represented in terms of the electromechanical constants of the SC, and $||\mu_m||$ has the structure similar to that of $||\mu_{SC}||$ and is represented in terms of the electromechanical constants of the 0–3 matrix. Following this approach and satisfying the aforementioned boundary conditions at the rod faces x_1=const and x_2=const, we form the $||M||$ matrix to be used in Eq.(1).

The $||K^{(SC)}||$ matrix from Eq.(1) contains elastic compliances (at E=const) $||s^{(SC),E}||$, piezoelectric coefficients $||d^{(SC)}||$ and dielectric permittivities $||\varepsilon^{(SC),\sigma}||$ (at σ=const). The $||K^{(m)}||$ matrix from Eq.(1) contains the similar set of the electromechanical constants of the 0–3 matrix, namely, $||s^{(m),E}||$, $||d^{(m)}||$ and $||\varepsilon^{(m),\sigma}||$. We note that this set differs from that in $||C^{(m)}||$ related also to the 0–3 matrix, and interrelations between $||s^{(m),E}||$ and $||c^{(m),E}||$, $||d^{(m)}||$ and $||e^{(m)}||$, $||\varepsilon^{(m),\sigma}||$ and $||\varepsilon^{(m),\xi}||$ are based on formulae [3,24] for piezoelectric media. The $||K^*||$ matrix from Eq.(1) has a structure similar to that of $||K^{(SC)}||$ and $||K^{(m)}||$, namely, $||K^*|| = \begin{pmatrix} ||s^{*E}|| & ||d^*||^t \\ ||d^*|| & ||\varepsilon^{*\sigma}|| \end{pmatrix}$, where effective elastic compliances $||s^{*E}||$, piezoelectric coefficients $||d^*||$ and dielectric permittivities $||\varepsilon^{*\sigma}||$ characterise the electromechanical properties of the 1–0–3 composite and depend on the volume fraction of SC rods r therein, the volume fraction of FC inclusions in the 0–3 matrix m_i and the aspect ratio of the FC

inclusion ρ_i. Elements of $||s^{*E}||$ $||d^*||$ and $||\varepsilon^{*\sigma}||$ are used at subsequent evaluations of the effective parameters $\Pi^*(r,m_i,\rho_i)$ of the 1–0–3 composite, and the relationships between Π^* and these matrices obey equations [3,24] that describe the piezoelecric medium. Thus, the effect studied in this work concentrates on changes in effective parameters of the 1–0–3 composite as a result of changes in the aspect ratio ρ_i in the 0–3 matrix at variations of volume fractions r and m_i.

Among the composite components of interest, the following materials are selected: (i) [001]-poled domain-engineered PMN–0.33PT SC as the main rod component in the 1–3 SC/polymer composite [1] (the full set of electromechanical constants of this SC is in Table 1), (ii) poled modified $PbTiO_3$ FC as the main component in the 0–3 matrix and (iii) the polymer is either araldite or polyurethane (Table 2) as the piezo-passive component in the 0–3 matrix. A PMN–0.33PT SC with a composition near the morphotropic phase boundary has been chosen since it exhibits a very high piezoelectric activity and moderate piezoelectric anisotropy [5], while the $PbTiO_3$-type FC is selected for its *contrasting* properties relative to the PMN–0.33PT SC, since it exhibits only a moderate piezoelectric activity, but has a large piezoelectric anisotropy [22]. Our choice is consistent with a selection of components for 1–3-type piezo-composites, wherein the component that is distributed continuously along one co-ordinate axis exhibits a high piezoelectric activity, and the component distributed continuously along three co-ordinate axes can be either piezo-passive or exhibiting a low piezoelectric activity [3,9]. As follows from experimental data [5,24], the coercive fields $E_c^{(n)}$ of the PMN–xPT SC (n=1) and $PbTiO_3$-type FC (n=2) satisfy the condition $E_c^{(1)} << E_c^{(2)}$. This condition enables an initial poling of the 0–3 matrix under a strong electric field with the subsequent poling of the SC rods in the composite (Fig.1,a) under a less intensive electric field. The subsequent poling may be carried out during the independent preparation of the system of aligned rods and the matrix [20].

Hereafter we analyse the following effective parameters $\Pi^*(r,m_i,\rho_i)$ of the 1–0–3 composite: piezoelectric coefficients g^*_{fl} found from the equation $d^*_{kl}=\varepsilon^{*\sigma}_{fk}\, g^*_{fl}$ for piezoelectric media [3,24], squared strain–voltage figures of merit

$$(Q^*_{33})^2=d^*_{33}\, g^*_{33} \text{ and } (Q^*_{31})^2=d^*_{31}\, g^*_{31}, \tag{2}$$

hydrostatic piezoelectric coefficients

$$d^*_h=d^*_{33}+2\,d^*_{31} \text{ and } g^*_h=g^*_{33}+2\,g^*_{31}, \tag{3}$$

and squared hydrostatic figure of merit

$$(Q^*_h)^2=d^*_h\, g^*_h. \tag{4}$$

It is assumed that electrodes applied to a composite sample (Fig.1,a) are perpendicular to the OX_3 axis. The squared figures of merit $(Q^*_{3j})^2$ from Eqs.(2) serve as an indicator of the sensor signal-to-noise ratio of the composite and its piezoelectric sensitivity [3,25] along the poling direction and on the direction perpendicular to the poling axis. Hydrostatic piezoelectric coefficients d^*_h and g^*_h from Eqs.(3) characterise the piezoelectric activity and sensitivity under hydrostatic loading of a piezoelectric element. $(Q^*_h)^2$ from Eq.(4) serves as a hydrostatic analog of $(Q^*_{3j})^2$ from Eqs.(2) and is often used [3,9,11] to characterise the piezoelectric sensitivity of the piezoelectric element under hydrostatic loading and to describe an effectiveness of a device as a hydrophone and as an actuator [15]. The squared figures of merit from Eqs.(2) and (4) are of interest for modern sensor networks, biomedical imaging and energy-harvesting devices [25–28] for the energy distribution as a result of mechanical loading along specific directions of the piezoelectric element.

3. Aspect-ratio effect on longitudinal and hydrostatic piezoelectric responses

In this section we discuss examples of the dependence of the effective parameters of the 1–0–3 composite on the aspect ratio ρ_i of the FC inclusions in the 0–3 matrix (see inset in Fig.1,a). Our calculations were performed using the full sets of electromechanical constants from Tables 1 and 2.

3.1. Local maxima of effective parameters versus the aspect ratio

The graphs in Fig.2 show that the local maxima $\Pi_{max}^{*}= \max\Pi^{*}(r,m_i,\rho_i)\,\big|_{\,m_i\,=const}$ strongly depend on the aspect ratio ρ_i of the FC inclusions even at relatively small volume fractions of FC ($m_i \leq 0.10$). From our evaluations, the local maxima $g^{*}_{33,\max}$ and $g^{*}_{h,\max}$ (Fig.2,a,d) are related to very small volume fractions of SC ($0.005<r<0.02$) at various ρ_i. The manufacture of a composite system at such low values of r may be challenging, although Choy et al. [29] were able to manufacture 1–3 FC/polymer composites with a FC rod volume fraction of approximately 0.033, 0.066, etc. We add that the formation of the regular structure of the piezo-active rods can be performed by means of a fixture [19] that is applicable in the wide range of volume fractions of the rods.

The local maxima $d^{*}_{h,\max}$ (Fig.2,c) are observed at relatively large volume fractions of SC ($0.4<r<0.5$). The difference in the SC volume-fraction dependence of the piezoelectric coefficients is a result of the important role of achieving a low dielectric permittivity $\varepsilon^{*\sigma}_{33}$ on the $g^{*}_{33}=d^{*}_{33}/\varepsilon^{*\sigma}_{33}$ and $g^{*}_{h}=d^{*}_{h}/\varepsilon^{*\sigma}_{33}$ piezoelectric coefficients (at $r<<1$), and the key role of the lateral piezoelectric effect (e.g., d^{*}_{31}) in the formation of d^{*}_{h} [see Eqs.(3)] in a wide r range. Local maxima $(Q^{*}_{33,\max})^2$ and $(Q^{*}_{h,\max})^2$ (Fig.2,b,e) are observed at $0.1<r<0.5$ and $0.07<r<0.2$, respectively. The influence of the non-monotonic behaviour of d^{*}_{h} and g^{*}_{h} on $(Q^{*}_{h,\max})^2$ is in agreement with Eq.(4), and the volume-fraction (r) range is located between those related to $g^{*}_{h,\max}$ (small volume fractions of SC) and $d^{*}_{h,\max}$ (moderate volume fractions of SC).

A correlation between $g^{*}_{33,\max}$ and $(Q^{*}_{33,\max})^2$ is observed (Fig.2,a,b) in a wide ρ_i range due to the relatively small volume fractions of SC ($r<<1$). Since the d^{*}_{33} piezoelectric coefficient, that influences $(Q^{*}_{33})^2$ in accordance with Eqs.(2), exhibits a monotonic dependence on r at various values of m_i and ρ_i the changes in $(Q^{*}_{33,\max})^2$ with ρ_i are mainly linked with changes in $g^{*}_{33,\max}$. The

local maxima of hydrostatic parameters with respect to r exhibit a similar behaviour in a wide ρ_i range (Fig.2,c–e): the hydrostatic piezoelectric response becomes more pronounced with increasing ρ_i, i.e., as the shape of the FC inclusions becomes highly oblate (see Fig.1,e and inset in Fig.1,a) and the 0–3 matrix becomes similar to a lamellar 2–2 composite.

We add that a 1–3 relaxor-ferroelectric SC/polymer composite (a case of $m_i = 0$ in our model) exhibits a series of non-monotonic volume-fraction dependences of effective parameters $\Pi^*(r)$, and no aspect-ratio effect can be detected in the 1–3 composite with a homogeneous polymer matrix. However for comparison, we give the following absolute maximum values of $\Pi^*(r)$ of the 1–3 PMN–0.33PT SC/polyurethane composite: $\max g_{33}^* = 825$ mV·m/N at $r = 0.011$, $\max[(Q_{33}^*)^2] = 242 \cdot 10^{-12}$ Pa^{-1} at $r = 0.109$, $\max[(Q_{31}^*)^2] = 36.9 \cdot 10^{-12}$ Pa^{-1} at $r = 0.135$, $\max d_h^* = 316$ pC/N at $r = 0.412$, $\max g_h^* = 201$ mV·m/N at $r = 0.011$, and $\max[(Q_h^*)^2] = 12.4 \cdot 10^{-12}$ Pa^{-1} at $r = 0.073$. Comparing the values of $\max\Pi^*(r)$ to the local-maximum values in Fig.2, we see that the aspect-ratio effect in the 1–0–3 composite leads to larger effective parameters $\Pi^*(r,m_i,\rho_i)$, and this improvement is observed even at relatively small volume fractions of the FC component ($m_i \leq 0.1$) within the matrix. The improved performance of the 1–0–3 composite is likely to be concerned with an important role of the *elastic* properties of the 0–3 matrix therein; this will be examined in Section 3.3 by considering a system of non-poled FC inclusions.

3.2. Aspect-ratio range $0.01<\rho_i<2$ and changes in the elastic anisotropy

An important example of the variation of the piezoelectric coefficient g_{33}^* and squared figures of merit $(Q_{3j}^*)^2$ with the aspect ratio ρ_i at small volume fractions of FC in the 0–3 matrix ($m_i = 0.05$) is shown in Fig.3. We see that there are large changes in the effective piezoelectric parameters of the 1–0–3 composite system at

$$0.01<\rho_i<2. \qquad (5)$$

In the aspect-ratio range (5) the shape of the FC inclusions in the 0–3 matrix changes from highly prolate (ρ_i<<1, Fig.1,d) to oblate (ρ_i>1, Fig.1,e). These changes in the microgeometry of the 0–3 matrix give rise to significant changes in its elastic properties and ratios of elastic compliances of the matrix $s_{1b}^{(m),E}/s_{kl}^{(m),E}$ (Fig.4,a,b) which have a strong influence on the piezoelectric properties and their anisotropy in the 1–0–3 composite as a whole. It is possible to observe a distinct correlation between the elastic compliance $s_{33}^{(m),E}$ of the 0–3 matrix (Fig.4,c) and the squared figure of merit $(Q_{33}^{*})^2$ of the composite (Fig.3,b). Such a correlation stems from the important role of the elastic compliance of the matrix $s_{33}^{(m),E}$ in the formation of the piezoelectric response of a 1–3 composite along the poling axis [3,12]. In the case of the 1–0–3 composite studied here the elastic anisotropy of the matrix leads to a strong link between $s_{33}^{(m),E}$ and $(Q_{33}^{*})^2$.

We add that the changes in $s_{1b}^{(m),E}/s_{kl}^{(m),E}$ are also appreciable, and the two ratios, namely $s_{11}^{(m),E}/s_{13}^{(m),E}$ and $s_{11}^{(m),E}/s_{33}^{(m),E}$, undergo major changes as a result of changes in the aspect-ratio (5) (see curves 2 and 3 in Fig.4,a,b). The $s_{11}^{(m),E}/s_{12}^{(m),E}$ ratio undergoes minor changes (see curve 1 in Fig. 4) while both $s_{11}^{(m),E}$ and $s_{12}^{(m),E}$ are related to the elastic response of the 0–3 matrix along the axes OX_1 and OX_2 (Fig.1,a) which are perpendicular to the poling direction. In our opinion, the behaviour of the aforementioned elastic compliances is a result of the dominating role of the highly anisotropic FC component in the 0–3 matrix. The change in $s_{13}^{(m),E}$ enables the composite engineer to vary the anisotropy of the piezoelectric coefficients d_{3j}^{*}, while the changes in $s_{33}^{(m),E}$ have an influence on g_{33}^{*} and $(Q_{33}^{*})^2$ even at volume fractions of SC r<<1.

3.3. Comparison of data

In this section we evaluate the effective parameters (2)–(4) of the 1–0–3 composite using different methods to calculate the effective properties of its 0–3 matrix. In the first case we calculate

the effective properties by means of FEM and then the effective properties of the 1–0–3 composite as a whole by means of the matrix method. In the second case EFM is used rather than FEM to determine the effective properties of the 0–3 matrix, and the matrix method is then applied to find the effective properties of the 1–0–3 composite. Example results are given for comparison in Table 3. It is seen that the effective parameters concerned with the longitudinal [g_{33}^* and $(Q_{33}^*)^2$], lateral [$(Q_{31}^*)^2$] and hydrostatic [d_h^*, g_h^* and $(Q_h^*)^2$] piezoelectric effects are in agreement when comparing data in Table 3. The largest relative error (δ= 10–11%) is related to squared figures of merit $(Q_{3j}^*)^2$ and $(Q_h^*)^2$. These parameters from Eqs. (2) and (4) combine the piezoelectric activity and sensitivity. As is known, maxima of $(Q_{3j}^*)^2$ and $(Q_h^*)^2$ are observed at relatively small volume fractions r of SC (approximately 0.1) due to a non-monotonic behaviour of g_{3j}^* and g_h^*, respectively. The location of $\max g_{33}^*$, $\min g_{31}^*$ and $\max g_h^*$ at $r<<1$ (as a rule, less than 0.05) strongly depends on the elastic and dielectric properties of the 0–3 matrix, and these properties are found using either EFM of FEM. As a consequence, differences between the EFM and FEM parameters of the 1–0–3 composite are detected especially near maxima of $(Q_{3j}^*)^2$ and $(Q_h^*)^2$, i.e., at r= 0.05 or 0.10, as given in Table 3.

Replacing araldite with a more compliant polyurethane (see elastic properties in Table 2) in the 0–3 matrix leads to an increase of all of the aforementioned effective parameters of the 1–0–3 composite (see Table 3). Such an effect is due to the more pronounced longitudinal and hydrostatic piezoelectric effects in a 1–3-type composite [30] that contains a more compliant matrix which allows a larger free deformation of the embedded piezoelectric rods. As follows from Table 3, g_{33}^* increases by about 1.2–1.4 times, and d_h^* increases by about 1.5–1.7 times in the presence of polyurethane in the 0–3 matrix. The use of the more compliant matrix has a significant influence on

the piezoelectric response of the composite along different co-ordinate axes. Table 3 contains data on the anisotropy of the squared figures of merit: we see that the relation $(Q_{33}^*)^2/(Q_{31}^*)^2 \approx 8–9$ holds at various values of r, m_i and ρ_i. A relatively large $(Q_{33}^*)^2/(Q_{31}^*)^2$ ratio is achieved due to the effect of the 0–3 matrix on the lateral piezoelectric response: the oblate FC inclusions in this matrix can weaken the piezoelectric coefficient d_{31}^* of the 1–0–3 composite.

Of particular interest is a case of a piezo-passive 0–3 matrix to examine the influence of the FC inclusion elastic properties on the composite performance. We now assume that the ceramic inclusions in a polymer medium surrounding the SC rods (Fig.1,a) have not been poled and, therefore, remain piezo-passive and isotropic. By varying the aspect ratio ρ_i of these inclusions it is possible to observe changes in the effective parameters of the 1–0–3 composite (Table 4), however these parameters become larger than those in the case of the poled (piezo-active) 0–3 matrix. This is a result of a decrease in the dielectric permittivity of the piezo-passive 0–3 matrix that leads to an appreciable decrease of $\varepsilon_{33}^{*\sigma}$ at relatively small SC volume fractions. Results shown in Table 4 suggest that the role of the elastic anisotropy in achieving high piezoelectric performance for the 1–0–3 composite is a dominant factor irrespective of the piezoelectric activity of its 0–3 matrix. Thus, during the manufacture of a 1–0–3 composite, there is no need to pole its 0–3 matrix under a relatively high electric field, as applied, for instance, to the $PbTiO_3$-type ceramic samples [24]. An incompleteness of the poling of the 0–3 matrix is avoided by this way, and a smaller dielectric permittivity $\varepsilon_{33}^{*\sigma}$ in the 1–0–3 composite favours its higher piezoelectric sensitivity.

As follows from Table 4, changes in the volume fraction of the ceramic component m_i in the 0–3 matrix give rise to weaker changes in the effective parameters of the composite in comparison to changes caused by the volume fraction of SC r. Such a behaviour is a result of the high piezoelectric activity of the SC rods and their parallel orientation along the poling axis: at such an

arrangement, even minor changes in r at r<<1 give rise to considerable changes in the piezoelectric performance and figures of merit [3,30].

The results of the present study are compared to data [29] on a 1–0–3 FC/FC/polyurethane composite where the highly piezo-active PCR-7M FC (a PZT-type composition) was used as a main component. Parameters that characterise the piezoelectric sensitivity of the 1–0–3 PCR-7M FC/PCR-7M FC/polyurethane composite [31] are g_{33}^{*}≈400 mV·m/N, g_{h}^{*}≈200 mV·m/N, and the piezoelectric coefficient that characterises the hydrostatic piezoelectric activity is d_{h}^{*}≈350 pC/N. These effective parameters are comparable to those related to the 1–0–3 SC/FC/polyurethane composite that consists of contrasting piezoelectric components. According to results [2], the maximum value of g_{33}^{*} determined for a 1–3 PMN–0.30PT/epoxy composite is 440 mV·m/N (at the volume fraction of SC r=0.018) and is comparable to values of g_{33}^{*} from Tables 3 and 4. According to data [8], a 1–3 composite based on PMN–PT SC is characterised by d_{h}^{*}=111 pC/N, g_{h}^{*}=37 mV·m/N and $(Q_{h}^{*})^{2}$=4.12·10^{-12}Pa^{-1}, i.e., these parameters are smaller than those given in Tables 3 and 4. We also add for comparison that a 1–3-type PZT FC / porous epoxy composite with a FC rod volume fraction 0.06 is characterised [32] by hydrostatic piezoelectric coefficients d_{h}^{*}=220 pC/N and g_{h}^{*}=228 mV·m/N at porosity levels in the matrix m_p=0.20 and d_{h}^{*}=284 pC/N, g_{h}^{*}=294 mV·m/N at m_p=0.40. The lower piezoelectric activity of the PZT FC component in comparison to that of the PMN–0.33PT SC and the elastic properties of the porous matrix lead to smaller values of d_{h}^{*} and g_{h}^{*} compared to the system studied in this work.

4. Conclusion

The present work reports original data and detailed analysis of the influence of an aspect-ratio effect for a high-performance 1–0–3 composite based on the relaxor-ferroelectric PMN–0.33PT SC. A significant feature of the studied composite is that elastic properties of its 0–3 matrix considerably

depend on the aspect ratio ρ_i of FC inclusions therein and influence the effective electromechanical properties of the 1–0–3 composite in wide aspect-ratio and volume-fraction ranges. This influence becomes important in the presence of two contrasting piezoelectric components, namely, a highly piezo-active PMN–0.33PT SC and highly anisotropic modified $PbTiO_3$ FC. The correlation between the longitudinal elastic compliance $s_{33}^{(m),E}$ of the 0–3 matrix and the squared figure of merit of the composite and the effect of ratios of elastic compliances $s_{1b}^{(m),E}/s_{pq}^{(m),E}$ on the piezoelectric response of the composite are observed at various values of ρ_i, especially at $0.01<\rho_i< 2$. As follows from comparison of data (see Tables 3 and 4), there is no need to pole the 0–3 matrix under a relatively high electric field, and the high piezoelectric sensitivity is achieved in the case of the non-poled 0–3 matrix with aligned ceramic inclusions.

In general, the electromechanical interaction between the highly piezo-active SC component and the anisotropic 0–3 matrix leads to the creation of high-performance 1–0–3 composite structures and enables the composite designer to vary its effective parameters by changing the volume fractions of both the SC and FC components and by changing the aspect ratio of FC inclusions. The large values of $g_{33}^{*}\sim10^2$ mV·m/N are of significant interest for sensor and receive-type transducer applications, and the large values of $d_h^{*}\sim10^2$ pC/N, $g_h^{*}\sim10^2$ mV·m/N and $(Q_h^{*})^2\sim10^{-11}$ Pa^{-1} make this composite attractive in hydrophone and related hydroacoustic applications. The large values of the squared figure of merit $(Q_{33}^{*})^2\sim10^{-10}$ Pa^{-1} and anisotropy $(Q_{33}^{*})^2/(Q_{31}^{*})^2\approx$8–9 are important for piezoelectric energy-harvesting applications. Moreover, the results on local maxima and non-monotonic behaviour of the effective parameters of the composite (Figs.2,3) and data on the elastic properties of the 0–3 matrix (Fig.4) can be of benefit for the further optimisation and exploitation of the piezoelectric sensitivity and hydrostatic characteristics of the studied 1–0–3 composite.

Acknowledgements. The authors would like to thank Prof.Dr. A.E. Panich, Prof.Dr. A.A. Nesterov and Prof.Dr. I.A. Parinov (Southern Federal University, Russia) and Prof.Dr. S.-H. Chang (National Kaohsiung Marine University, Taiwan, ROC) for their constant interest in the research problem. Prof.Dr. C.R. Bowen acknowledges funding from the European Research Council under the European Union's Seventh Framework Programme (FP/2007-2013) / ERC Grant Agreement no.320963 on Novel Energy Materials, Engineering Science and Integrated Systems (NEMESIS). The work has been performed using the equipment of the Centre of Collective Use "High Technologies" at the Southern Federal University within the framework of the project RFMEFI59414X0002. The research subject is also concerned with the Programme Supporting the Research at the Southern Federal University.

References

[1] K. Ren, Y. Liu, X. Geng, H.F. Hofmann, Q.M. Zhang, Single crystal PMN-PT/epoxy 1–3 composite for energy-harvesting application, IEEE Trans.Ultrason., Ferroelectr.Freq.Contr.53 (2006) 631–638.

[2] F. Wang, C. He, Y. Tang, Single crystal $0.7Pb(Mg_{1/3}Nb_{2/3})O_3–0.3PbTiO_3$ epoxy 1–3 piezoelectric composites prepared by the lamination technique, Mater.Chem.Phys.105 (2007) 273–277.

[3] V.Yu. Topolov, P. Bisegna, C.R. Bowen, Piezo-active Composites. Orientation Effects and Anisotropy Factors, Springer, Berlin, Heidelberg, 2014.

[4] L. Li, S. Zhang, Z. Xu, X. Geng, F. Wen, J. Luo, T.R. Shrout, Hydrostatic piezoelectric properties of [011] poled $Pb(Mg_{1/3}Nb_{2/3})O_3–PbTiO_3$ single crystals and 2–2 lamellar composites, Appl.Phys.Lett.104 (2014) 032909–3 p.

[5] R. Zhang, B. Jiang, W. Cao, Elastic, piezoelectric, and dielectric properties of multidomain $0.67Pb(Mg_{1/3}Nb_{2/3})O_3–0.33PbTiO_3$ single crystals, J.Appl.Phys.90 (2001) 3471–3475.

[6] R. Zhang, B. Jiang, W. Cao, A. Amin, Complete set of material constants of $0.93Pb(Zn_{1/3}Nb_{2/3})O_3–0.07PbTiO_3$ domain engineered single crystal, J.Mater.Sci.Lett.21 (2002) 1877–1879.

[7] S. Zhang, G. Liu, W. Jiang, J. Luo, W. Cao, T.R. Shrout, Characterization of single domain $Pb(In_{0.5}Nb_{0.5})O_3–Pb(Mg_{1/3}Nb_{2/3})O_3–PbTiO_3$ crystals with monoclinic phase, J.Appl.Phys.110 (2011) 064108–8 p.

[8] S. Zhang, F. Li, High performance ferroelectric relaxor-$PbTiO_3$ single crystals: Status and perspective, J.Appl.Phys.111 (2012) 031301–50 p.

[9] E.K. Akdogan, M. Allahverdi, A. Safari, Piezoelectric composites for sensor and actuator applications, IEEE Trans.Ultrason., Ferroelectr.Freq.Contr.52 (2005) 746–775.

[10] R.E. Newnham, D.P. Skinner, L.E. Cross, Connectivity and piezoelectric-pyroelectric composites, Mater.Res.Bull.13 (1978) 525–536.

[11] L.V. Gibiansky, S. Torquato, On the use of homogenization theory to design optimal piezocomposites for hydrophone applications, J.Mech.Phys.Solids 45 (1997) 689–708.

[12] V.Yu. Topolov, A.E. Panich, Problem of piezoelectric sensitivity of 1–3-type composites based on ferroelectric ceramics, Ferroelectrics 392 (2009) 107–119.

[13] V.Yu. Topolov, A.V. Turik, Porous piezoelectric composites with extremely high reception parameters, Tech.Phys.46 (2001) 1093–1100.

[14] Y. Hirata, T. Numazawa, H. Takada, Effect of aspect ratio of lead zirconate titanate on 1–3 piezoelectric composite properties, Jap.J.Appl.Phys.36 (1997) 6062–6064.

[15] J. Bennett, G. Hayward, Design of 1–3 piezocomposite hydrophones using finite element analysis, IEEE Trans.Ultrason., Ferroelectr.Freq.Contr.44 (1997) 565–574.

[16] W. Cao, Q.M. Zhang, L.E. Cross, Theoretical study on the static performance of piezoelectric ceramic–polymer composites with 2–2 connectivity, IEEE Trans.Ultrason.,Ferroelectr. Freq.Contr.40 (1993) 103–109.

[17] J.H. Huang, W.-S. Kuo, Micromechanics determination of the effective properties of piezoelectric composites containing spatially oriented short fibers, Acta Mater.44 (1996) 4889–4898.

[18] S.A. Wilson, G.M. Maistros, R. Whatmore, Structure modification of 0–3 piezoelectric ceramic/polymer composites through dielectrophoresis, J.Phys.D:Appl.Phys.38 (2005) 175–182.

[19] K.A. Klicker, J.V. Biggers, R.E. Newnham, Composites of PZT and epoxy for hydrostatic transducer applications, J.Am.Cer.Soc.64 (1981) 5–9.

[20] C. Richard, Étude expérimentale et théorique de composites piézoélectriques de connectivité 1.3.1 pour hydrophone, Thesis, Institut National des Sciences Appliquées de Lyon, Lyon, 1992.

[21] COMSOL, Inc. COMSOLMultiphysics^{TM}User's Guide(version 4.4, 2014), http://www.comsol.com

[22] S. Ikegami, I. Ueda, T. Nagata, Electromechanical properties of $PbTiO_3$ ceramics containing La and Mn, J.Acoust.Soc.Am.50 (1971) 1060–1066.

[23] F. Levassort, M. Lethiecq, C. Millar, L. Pourcelot, Modeling of highly loaded 0–3 piezoelectric composites using a matrix method, IEEE Trans.Ultrason.,Ferroelectr.Freq. Contr.45 (1998) 1497–1505.

[24] Y. Xu, Ferroelectric Materials and Their Applications, North-Holland, Amsterdam, London, New York, Toronto, 1991.

[25] S. Priya, Criterion for material selection in design of bulk piezoelectric energy harvesters, IEEE Trans.Ultrason.,Ferroelectr.Freq.Contr.57 (2010) 2610–2612.

[26] K. Uchino, T. Ishii, Energy flow analysis in piezoelectric energy harvesting systems, Ferroelectrics 400 (2010) 305–320.

[27] Y. Yan, K.-H. Cho, D. Maurya, A. Kumar, S. Kalinin, A. Khachaturyan, S. Priya, Giant energy density in [001]-textured $Pb(Mg_{1/3}Nb_{2/3})O_3$–$PbZrO_3$–$PbTiO_3$ piezoelectric ceramics. Appl.Phys.Lett.102 (2013) 042903–3 p.

[28] M. Sakthivel, A. Arockiarajan, An effective matrix poling characteristics of 1–3–2 piezoelectric composites, Sens.Actuators A: Phys.167 (2011) 34–43.

[29] S.H. Choy, H.L.W. Chan, M.W. Ng, P.C.K. Liu, Study of 1–3 PZT fibre/epoxy composites with low volume fraction of ceramics, Integr.Ferroelectr.63 (2004) 109–115.

[30] A.A. Grekov, S.O. Kramarov, A.A. Kuprienko, Effective properties of a transversely isotropic piezoelectric composite with cylindrical inclusions, Mech.Compos.Mater.25 (1989) 54–61.

[31] V.Yu. Topolov, C.R. Bowen, S.E. Filippov, High performance of novel 1–3-type composites based on ferroelectric PZT-type ceramics, Ferroelectrics 430 (2012) 92–97.

[32] M.J. Haun, R.E. Newnham, An experimental and theoretical study of 1–3 and 1–3–0 piezoelectric PZT-polymer composites for hydrophone applications, Ferroelectrics 68 (1986) 123–139.

Table 1. Room-temperature elastic compliances s_{ab}^{E} (in 10^{-12} Pa^{-1}), piezoelectric coefficients d_{fl} (in pC/N) and relative dielectric permittivities $\varepsilon_{rr}^{\sigma}/\varepsilon_0$ of [001]-poled domain-engineered PMN–0.33PT SC (4*mm* symmetry) [5]

s_{11}^{E}	s_{12}^{E}	s_{13}^{E}	s_{33}^{E}	s_{44}^{E}	s_{66}^{E}	d_{31}	d_{33}	d_{15}	$\varepsilon_{11}^{\sigma}/\varepsilon_0$	$\varepsilon_{33}^{\sigma}/\varepsilon_0$
69.0	–11.1	–55.7	119.6	14.5	15.2	–1330	2820	146	1600	8200

Table 2. Room-temperature elastic moduli c_{ab}^{E} (in 10^{10} Pa), piezoelectric coefficients e_{ij} (in C/m^2) and dielectric permittivities $\varepsilon_{pp}^{\xi}/\varepsilon_0$ of FC and polymer components

Compo-nent	c_{11}^{E}	c_{12}^{E}	c_{13}^{E}	c_{33}^{E}	c_{44}^{E}	e_{31}	e_{33}	e_{15}	$\varepsilon_{11}^{\xi}/\varepsilon_0$	$\varepsilon_{33}^{\xi}/\varepsilon_0$
Modified $PbTiO_3$ FC [22]	14.33	3.220	2.413	13.16	5.587	0.4584	6.499	5.923	210	140
Araldite [23]	0.78	0.44	0.44	0.78	0.17	0	0	0	4.0	4.0
Polyur-ethane [11]	0.442	0.26	0.26	0.442	0.091	0	0	0	3.5	3.5

Table 3. Comparison of effective parameters calculated for the 1–0–3 PMN–0.33PT SC/modified $PbTiO_3$ FC/polymer composite using either the FEM (Π^*_{FEM}) or EFM (Π^*_{EFM}) to evaluate the electromechanical properties of the 0–3 matrix. Relative error $\delta = (|\Pi^*_{FEM} - \Pi^*_{EFM}| / \Pi^*_{FEM}) \cdot 100\%$ is given near the effective parameters Π^*_{EFM}

Evaluation method for 0–3 matrix properties	ρ_i	m_i	r	g^*_{33}, mV·m/N	$(Q^*_{33})^2$, 10^{-12} Pa^{-1}	$(Q^*_{31})^2$, 10^{-12} Pa^{-1}	d^*_h, pC/N	g^*_h, mV·m/N	$(Q^*_h)^2$, 10^{-12} Pa^{-1}
1–0–3 PMN–0.33PT SC/modified $PbTiO_3$ FC/araldite composite									
FEM	1.5	0.05	0.05	433	96.6	12.3	60.2	117	7.03
	2.0	0.05	0.05	433	96.4	12.1	61.3	119	7.30
	2.5	0.05	0.05	432	95.7	11.8	62.3	121	7.57
	1.5	0.10	0.05	406	81.3	9.84	57.7	117	6.75
	2.0	0.10	0.05	405	80.6	9.45	59.5	121	7,22
	2.5	0.10	0.05	403	79.2	8.98	61.0	125	7.65
	1.5	0.05	0.10	291	126	16.6	111	74.6	8.27
	2.0	0.05	0.10	291	126	16.3	113	76.1	8.58
	2.5	0.05	0.10	291	125	15.9	115	77.6	8.90
	1.5	0.10	0.10	281	110	13.8	107	76.8	8,21
	2.0	0.10	0.10	281	109	13.3	110	79.6	8.77
	2.5	0.10	0.10	280	108	12.7	113	82.3	9.30
EFM	1.5	0.05	0.05	438 (1.2%)	98.8 (2.3%)	12.4 (0.8%)	61.7 (2.5%)	120 (2.6%)	7.39 (5.1%)
	2.0	0.05	0.05	439 (1.4%)	99.2 (2.9%)	12.2 (0.8%)	63.2 (3.1%)	123 (3.4%)	7.77 (6.4%)
	2.5	0.05	0.05	439 (1.6%)	99.1 (3.6%)	12.0 (1.7%)	64.3 (3.2%)	125 (3.3%)	8.06 (6.5%)
	1.5	0.10	0.05	418 (3.0%)	86.8 (6.8%)	10.4 (5.7%)	60.4 (4.7%)	121 (3.4%)	7.33 (8.6%)
	2.0	0.10	0.05	420 (3.7%)	87.5 (8.6%)	10.2 (7.9%)	62.9 (5.7%)	127 (5.0%)	7.97 (10%)
	2.5	0.10	0.05	420 (4.2%)	87.5 (10%)	9.88 (10%)	64.9 (6.4%)	131 (4.8%)	8.50 (11%)
	1.5	0.05	0.10	293 (0.7%)	128 (1.6%)	16.6 (0%)	113 (1.8%)	76.0 (1.9%)	8.61 (4.1%)
	2.0	0.05	0.10	293 (0.7%)	128 (1.6%)	16.4 (0.6%)	116 (2.7%)	77.8 (2.2%)	9.04 (5.4%)
	2.5	0.05	0.10	293 (0.7%)	128 (2.3%)	16.1 (1.3%)	118 (2.6%)	79.3 (2.2%)	9.37 (5.3%)
	1.5	0.10	0.10	285 (1.4%)	115 (4.5%)	14.4 (4.3%)	111 (3.7%)	78.5 (2.2%)	8.47 (3.2%)
	2.0	0.10	0.10	286 (1.8%)	116 (6.4%)	14.0 (5.3%)	116 (5.5%)	81.6 (2.5%)	9.48 (8.1%)
	2.5	0.10	0.10	286 (2.1%)	116 (7.4%)	13.6 (7.1%)	120 (6.2%)	84.3 (2.4%)	10.1 (8.6%)

Table 3 (*continued*)

1–0–3 PMN–0.33PT SC/modified $PbTiO_3$ FC/polyurethane composite									
FEM	1.5	0.05	0.05	549	212	27.7	98.5	140	13.8
	2.0	0.05	0.05	549	212	27.2	100	143	14.4
	2.5	0.05	0.05	548	210	26.5	102	146	15.0
	1.5	0.10	0.05	525	182	22.6	95.2	144	13.7
	2.0	0.10	0.05	524	180	21.6	98.5	150	14.8
	2.5	0.10	0.05	522	177	20.4	101	156	15.8
	1.5	0.05	0.10	332	235	31.5	171	80.5	13.8
	2.0	0.05	0.10	332	235	30.9	175	82.3	14.4
	2.5	0.05	0.10	332	233	30.2	178	84.2	15.0
	1.5	0.10	0.10	325	209	26.7	168	84.5	14.2
	2.0	0.10	0.10	324	207	25.6	173	87.9	15.2
	2.5	0.10	0.10	324	204	24.4	178	91.4	16.3
EFM	1.5	0.05	0.05	553 (0.7%)	217 (2.4%)	28.1 (1.4%)	101 (2.5%)	143 (2.1%)	14.4 (4.3%)
	2.0	0.05	0.05	553 (0.7%)	218 (2.8%)	27.5 (1.1%)	104 (4.0%)	147 (2.8%)	15.3 (6.3%)
	2.5	0.05	0.05	553 (0.9%)	218 (3.8%)	27.0 (1.9%)	107 (4.9%)	150 (2.7%)	16.1 (7.3%)
	1.5	0.10	0.05	531 (1.1%)	194 (6.6%)	23.7 (4.9%)	100 (5.0%)	148 (2.8%)	14.8 (8.0%)
	2.0	0.10	0.05	536 (2.3%)	195 (8.3%)	23.0 (6.5%)	105 (6.6%)	155 (3.3%)	16.3 (10%)
	2.5	0.10	0.05	536 (2.7%)	195 (10%)	22.2 (8.8%)	109 (7.9%)	161 (3.2%)	17.5 (11%)
	1.5	0.05	0.10	333 (0.3%)	240 (2.1%)	31.8 (1.0%)	176 (2.9%)	81.8 (1.6%)	14.4 (4.3%)
	2.0	0.05	0.10	334 (0.6%)	240 (2.1%)	31.2 (6.5%)	181 (3.4%)	84.0 (2.1%)	15.2 (5.6%)
	2.5	0.05	0.10	334 (0.6%)	240 (3.0%)	30.6 (1.3%)	185 (3.9%)	86.1 (2.3%)	16.0 (6.3%)
	1.5	0.10	0.10	328 (0.9%)	219 (4.8%)	27.7 (3.7%)	176 (4.8%)	86.0 (1.8%)	15.1 (6.3%)
	2.0	0.10	0.10	328 (1.2%)	220 (6.3%)	26.8 (4.7%)	184 (6.4%)	90.0 (2.4%)	16.6 (9.2%)
	2.5	0.10	0.10	328 (1.2%)	220 (7.8%)	26.0 (6.6%)	191 (7.3%)	93.4 (2.2%)	17.8 (9.2%)

Table 4. Effective parameters calculated for the 1–0–3 PMN–0.33PT SC/modified $PbTiO_3$ ceramic/polyurethane composite in a case of a piezo-passive 0–3 matrix[a]

ρ_i	m_i	r	g_{33}^*, mV·m/N	$(Q_{33}^*)^2$, 10^{-12} Pa^{-1}	$(Q_{31}^*)^2$, 10^{-12} Pa^{-1}	d_h^*, pC/N	g_h^*, mV·m/N	$(Q_h^*)^2$, 10^{-12} Pa^{-1}
1.5	0.05	0.05	553	218	28.1	102	143	14.5
2.0	0.05	0.05	554	218	27.5	105	147	15.4
2.5	0.05	0.05	554	218	27.0	107	150	16.1
1.5	0.10	0.05	535	194	23.7	101	148	14.9
2.0	0.10	0.05	536	185	23.0	105	155	16.3
2.5	0.10	0.05	536	195	22.2	109	161	17.6
1.5	0.05	0.10	333	240	31.7	177	81.9	14.5
2.0	0.05	0.10	334	240	31.2	182	84.1	15.3
2.5	0.05	0.10	334	240	30.6	186	86.1	16.0
1.5	0.10	0.10	328	220	27.7	176	86.2	15.2
2.0	0.10	0.10	328	221	26.8	195	90.2	16.6
2.5	0.10	0.10	328	220	25.9	191	93.5	17.9

[a] Electromechanical properties of the 0–3 matrix were evaluated by EFM

List of figure captions to the paper SNA-D-14-01357 "New aspect-ratio effect in three-component composites for piezoelectric sensor, hydrophone and energy-harvesting applications"

by V Yu Topolov, C R Bowen and P Bisegna

Fig. 1. Schematic of the 1–0–3 relaxor-ferroelectric SC/FC/polymer composite (a), the arrangement of SC rods with square bases in a surrounding medium (b), the arrangement of spheroidal FC inclusions in a polymer matrix (c), and meshes of the 0–3 composite matrix at $0< \rho_i< 1$ (d, for finite element modelling) and at $\rho_i> 1$ (e, for finite element modelling). In Fig.1,a–c ($X_1X_2X_3$) is a rectangular co-ordinate system concerned with the composite sample. $\boldsymbol{P}_s^{(1)}$ is the spontaneous polarisation of the SC rod, r and $1–r$ are volume fractions of the SC rods and the surrounding 0–3 matrix, respectively, m_i is the volume fraction of the isolated FC inclusions in the polymer medium, and a_1 and a_3 are semi-axes of each FC inclusion.

Fig. 2. Aspect-ratio (ρ_i) dependence of local maxima of the piezoelectric coefficient $g^*_{33,max}$ (a, in mV·m/N), squared figure of merit $(Q^*_{33,max})^2$ (b, in 10^{-12} Pa^{-1}), hydrostatic piezoelectric coefficients $d^*_{h,max}$ (c, in pC/N) and $g^*_{h,max}$ (d, in mV·m/N), and hydrostatic squared figure of merit $(Q^*_{h,max})^2$ (e, in 10^{-12} Pa^{-1}) of the 1–0–3 PMN–0.33PT SC/modified $PbTiO_3$ FC/polyurethane composite at the volume fraction of FC inclusions m_i=const. At the first stage of averaging, electromechanical properties of the 0–3 matrix were evaluated by EFM.

Fig. 3. Aspect-ratio (ρ_i) dependence of the piezoelectric coefficient g^*_{33} and hydrostatic piezoelectric coefficient g^*_h (a, in mV·m/N), and squared figures of merit $(Q^*_{3j})^2$ (b, in 10^{-12} Pa^{-1}) of the 1–0–3 PMN–0.33PT SC/modified $PbTiO_3$ FC/polyurethane composite at volume fractions

m_i=const (FC inclusions in the 0–3 matrix) and r=const (SC rods in the composite). At the first stage of averaging, electromechanical properties of the 0–3 matrix were evaluated by EFM.

Fig. 4. Aspect-ratio (ρ_i) dependence of ratios of elastic compliances $s_{1b}^{(m),E} / s_{kl}^{(m),E}$ (a and b) and the elastic compliance $s_{33}^{(m),E}$ (c, in 10^{-10} Pa^{-1}) of the 0–3 modified $PbTiO_3$ FC/polyurethane composite matrix. Electromechanical properties were evaluated by EFM.

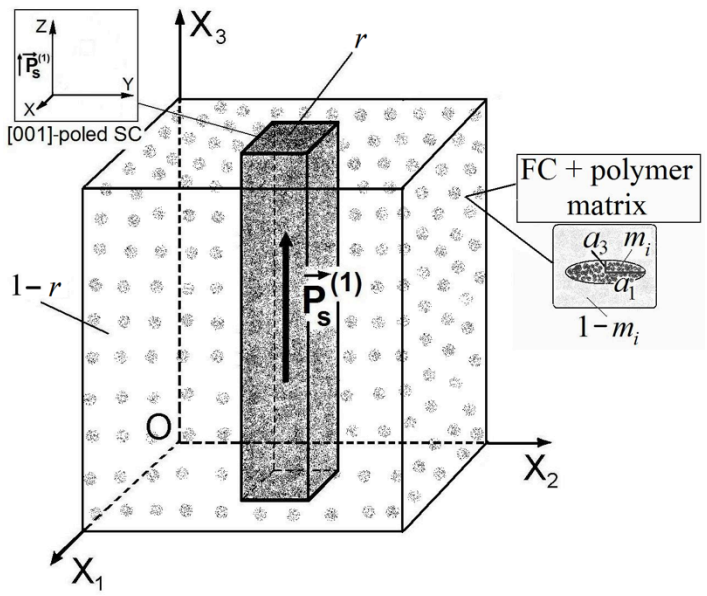

a

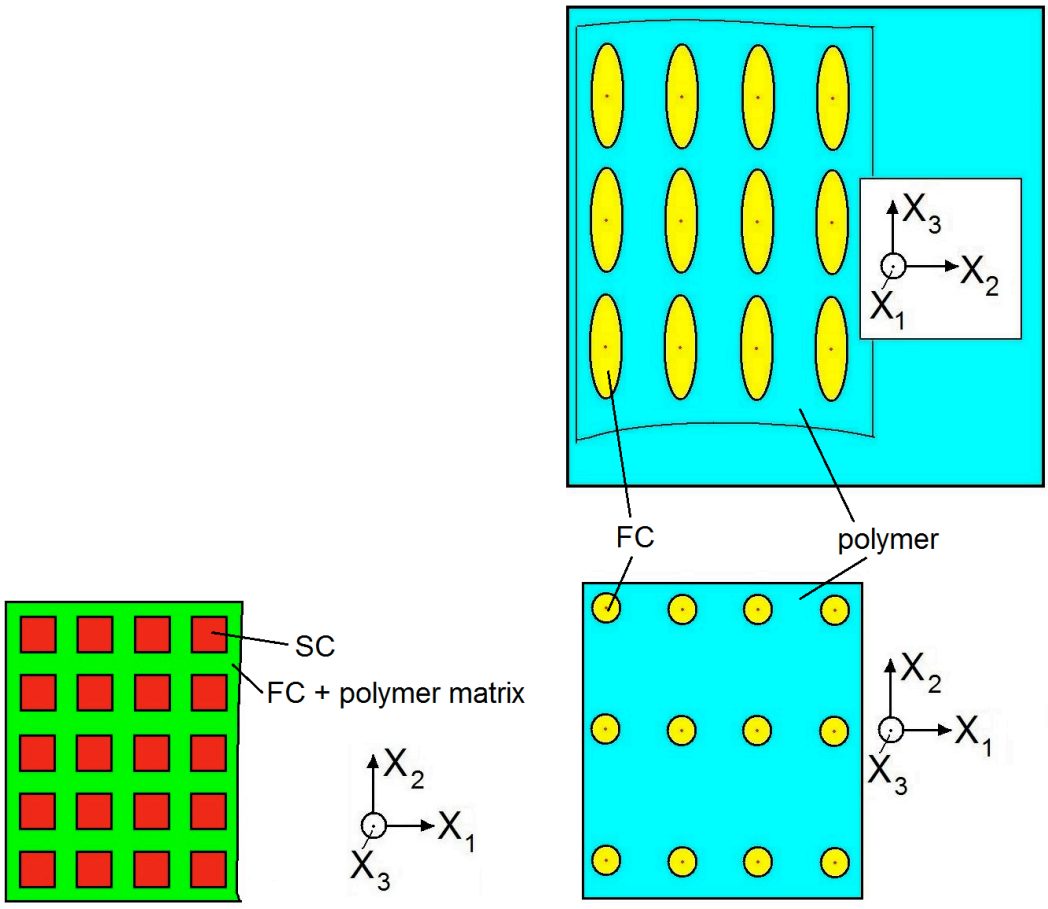

b c

Fig. 1 (*continued*)

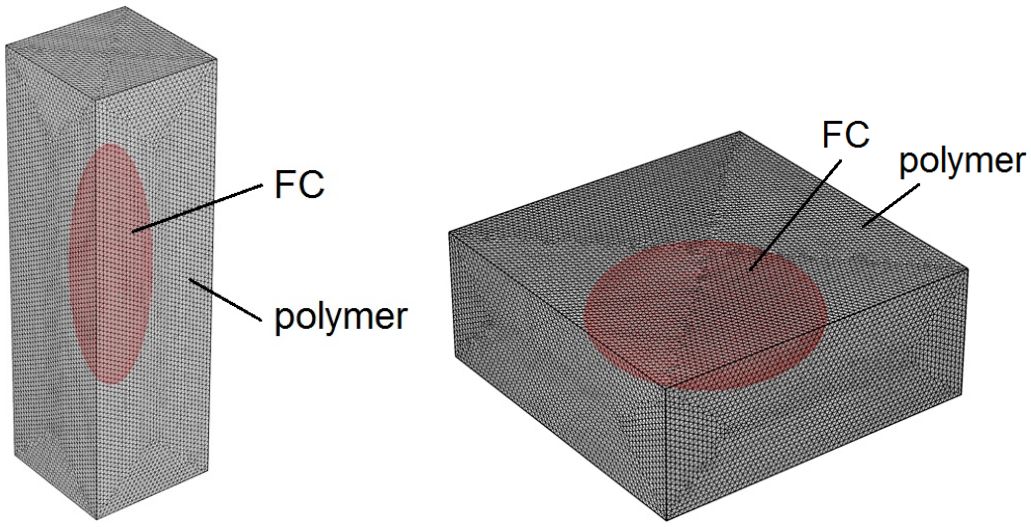

d e

Fig. 1

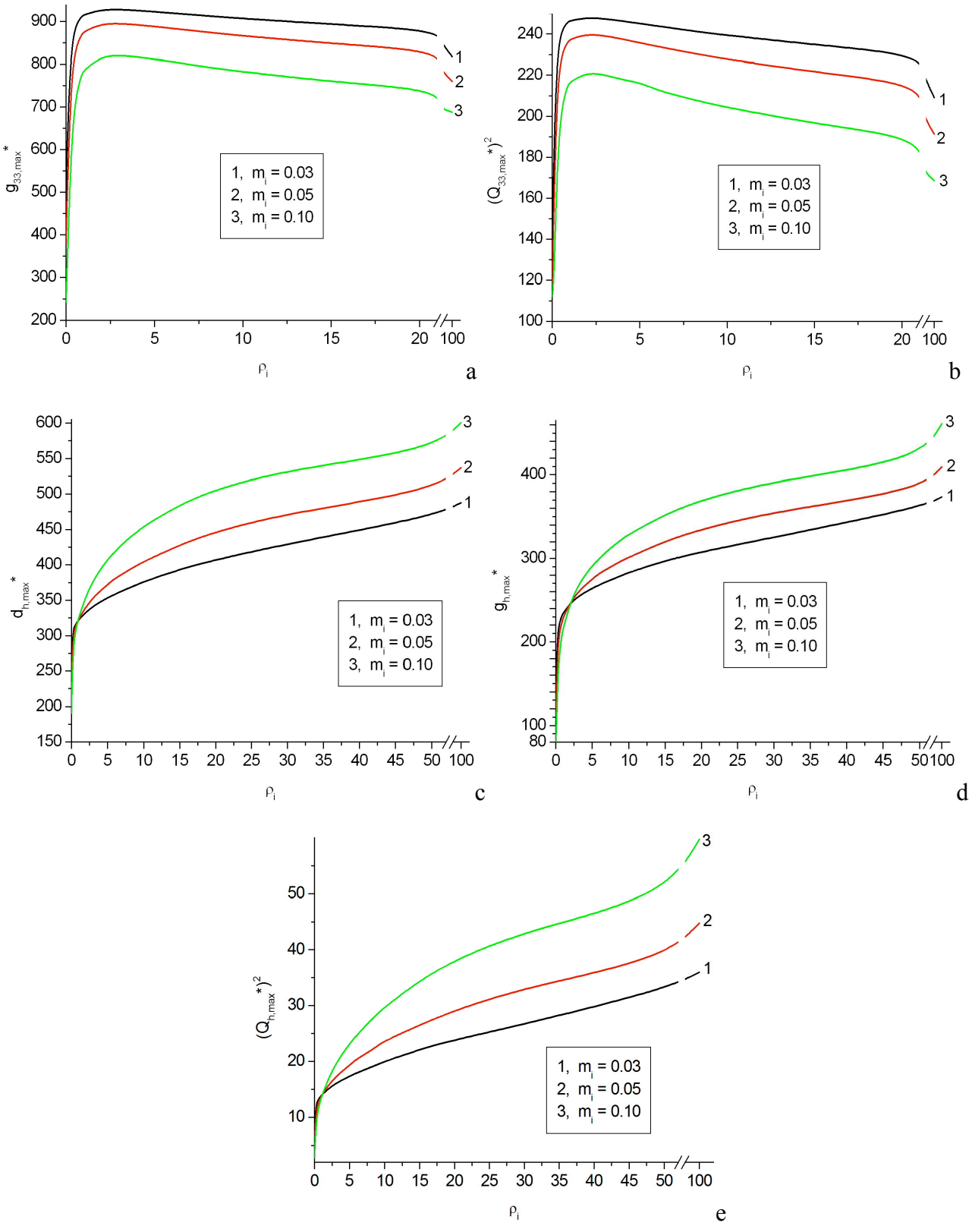
$g_{33,max}^*$
$(Q_{33,max}^*)^2$
$d_{h,max}^*$
$g_{h,max}^*$
$(Q_{h,max}^*)^2$
ρ_i
1, m_i = 0.03
2, m_i = 0.05
3, m_i = 0.10
a
b
c
d
e

Fig. 2

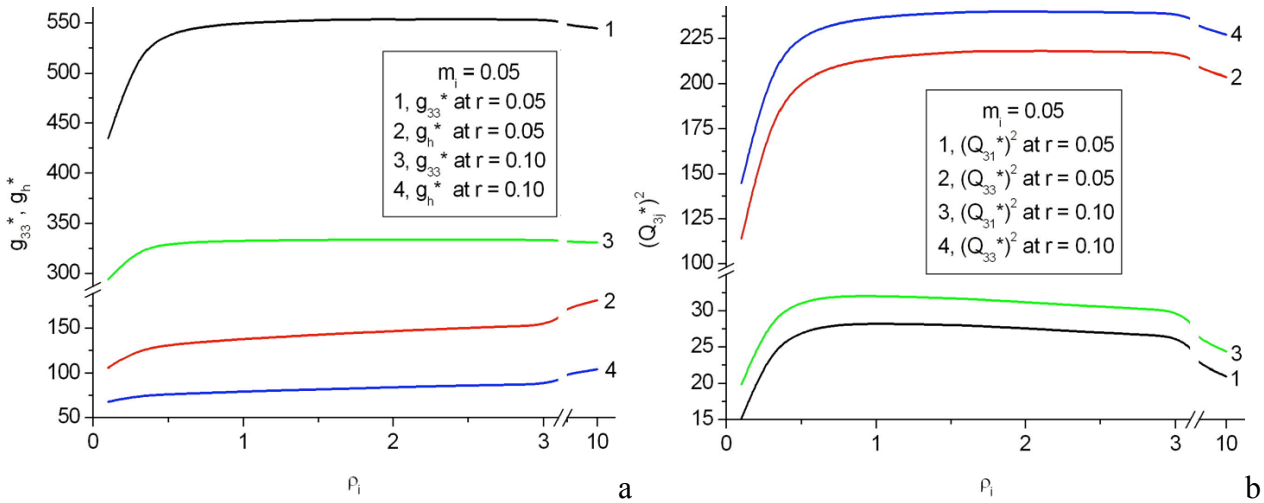
m_i = 0.05
1, g_33* at r = 0.05
2, g_h* at r = 0.05
3, g_33* at r = 0.10
4, g_h* at r = 0.10
g_33*, g_h*
ρ_i
a
m_i = 0.05
1, (Q_31*)^2 at r = 0.05
2, (Q_33*)^2 at r = 0.05
3, (Q_31*)^2 at r = 0.10
4, (Q_33*)^2 at r = 0.10
(Q_3j*)^2
ρ_i
b

Fig. 3

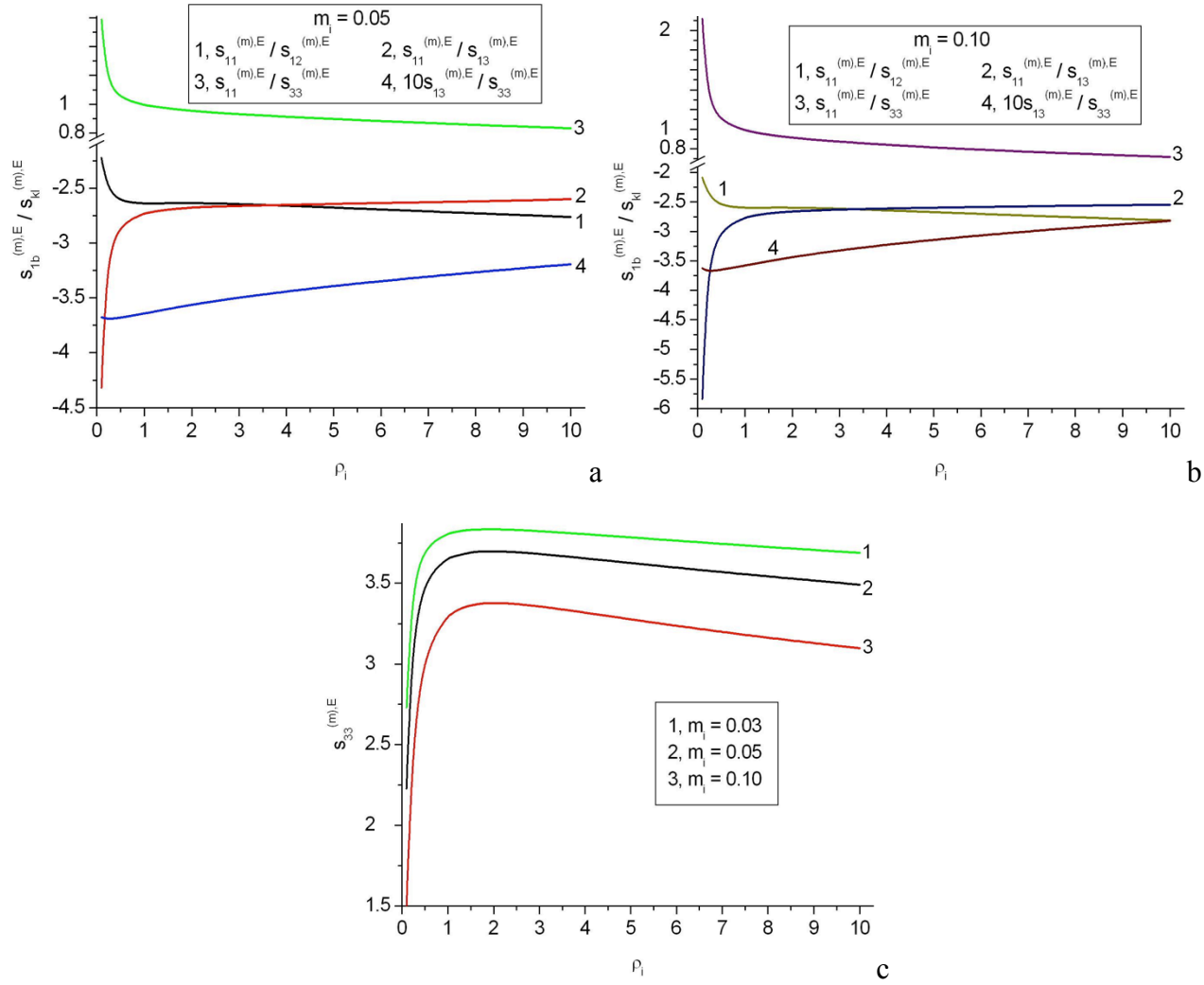
m_i = 0.05
1, s_11^(m),E / s_12^(m),E
2, s_11^(m),E / s_13^(m),E
3, s_11^(m),E / s_33^(m),E
4, 10s_13^(m),E / s_33^(m),E
s_1b^(m),E / s_kl^(m),E
ρ_i
a
m_i = 0.10
1, s_11^(m),E / s_12^(m),E
2, s_11^(m),E / s_13^(m),E
3, s_11^(m),E / s_33^(m),E
4, 10s_13^(m),E / s_33^(m),E
s_1b^(m),E / s_kl^(m),E
ρ_i
b
1, m_i = 0.03
2, m_i = 0.05
3, m_i = 0.10
s_33^(m),E
ρ_i
c

Fig. 4